Detonation Simulations for the CE80+ Nuclear Power Plant Design

J. E. Shepherd
GALCIT, 105-50
California Institute of Technology
Pasadena, CA 91125

July 2, 1994

Prepared for the U. S. Nuclear Regulatory Commission
under contract ERI-NRC-02-92-046.

Executive Summary

One-dimensional detonation simulations and simplified structural response computations have been carried out to assess the significance of the detonation of local regions of the CE80+ containment. For a cloud size that is 15% of the upper dome volume and computed SB LOCA conditions, the first reflected shock results in a peak pressure of 8.6 bar on the containment when the initial containment pressure of 2.37 bar is accounted for. The peak reflected pressure increases as the cloud size is increased, up to a maximum value of 14.4 bar for a cloud that occupies the entire hemisphere modeling the upper dome of the containment.

The ultimate capacity of the shell has been estimated to be 12.8 bar at a temperature of 393 K. The equivalent static pressures computed from the single-degree-of-freedom structural model are comparable to this pressure except in case 2, which had an equivalent static pressure of 19.2 bar. However, even in this case, only a modest amount of permanent deformation would be expected since tensile failure is not expected until a static pressure of 88 bar.

We conclude that: Local detonations with realistic quantities of hydrogen produce structural loads that are comparable with the ultimate capacity but far below the tensile failure limit of the steel shell. The interaction of the detonation with the cloud boundary and the decay of the shock wave due to the expansion wave are significant in determining peak pressures and structural deflections. An optimum cloud size appears to exist for generating the maximum deflection of the structure. The maximum deflection occurs due the interaction of the secondary shock waves with the structural oscillations.

Finally, these computations indicate that computing structural deformation from blast loading can involve subtle effects that requires careful evaluation. Simple engineering correlations developed for external blast must be used very cautiously. If more realistic computations with multidimensional geometries are used for the gas dynamic portion, there should be a comparable increase in the sophistication of the structural computation.

Contents

List of Figures

List of Tables

1 Introduction

One-dimensional numerical simulations of detonation propagation in the CE80+ containment have been performed. These simulations only consider the problem of detonation propagation in the region of the containment above the operating deck. The purpose of these calculations is to determine loads from "local" detonations, that is, detonation of a smaller region within the containment. The upper portion of the containment is idealized as a hemisphere in these preliminary computations. The fraction of volume occupied by the cloud has been considered as a parameter in these computations and was varied from 15% to 100% .

The results of the simulations are pressure and impulse histories at selected locations within the containment. The implication of these results for containment integrity are assessed using a simple single-degree-of-freedom model for a spherical shell. The maximum shell deflection is calculated by direct integration of the structural response equation using the computed loading. Shell radial deflections as a function of time are presented for each case and the equivalent static loadings for the maximum deflection are tabulated. These results indicate that the load is in a mixed regime that requires a time-dependent analysis in order to estimate structural deflection.

2 Initial Conditions

If the hydrogen released in an accident is completely mixed with the contents of the containment, then a very low concentration of hydrogen will result. Typically, such a mixture can not be detonated and in some cases, will not even burn. In order for the mixture to be detonable, the composition must fall within a limited range. This range has been estimated (Shepherd 1993) based on the previous experimental and simulation studies on hydrogen combustion and is shown in Fig. 1. Accident simulations for the CE80+ predict hydrogen concentrations of 5% and steam concentrations of 50% if the containment is well mixed. This is close to the lean flammability limit. Therefore, if a detonation occurs, it must be due to a local high concentration of hydrogen associated with incomplete mixing. Such a local concentration of hydrogen could result in a"local" detonation.

In order to examine the problem of local detonation, we imagine that the hydrogen released in the accident will all be within a small region or "cloud." CONTAIN calculations carried out at BNL for a SBLOCA situation (dry cavity, no igniters, 62% total metal-water reaction) in the CE80+ were analyzed to obtain typical containment atmosphere conditions for the detonation simulations. The total amount of hydrogen computed in these simulations has been used to determine the size and composition of localized clouds within the containment. Specifically, we used the composition given at 12840 s, which resulted in a containment temperature of 394 K, a pressure of 237 kPa and a composition shown in Table 1.

The cloud composition was calculated by assuming that this total amount of hydrogen (computed from a free volume of 3.34 $\times 10^6$ ft^3) was concentrated into a smaller fraction

of the total volume. Note that the air and steam fractions proportionately decrease as the hydrogen fraction increases with decreasing cloud size. The relationship between cloud size and composition is shown in Table 2 and Fig. 2. For the purpose of the present computations, the small amount of CO and the minor constituents of air (CO_2, Ar) have been lumped into the N_2 concentration.

Comparing these compositions to the detonability diagram of Fig. 1, a cloud volume of 15% of the total free volume was been chosen as the test case for the detonation calculations. The composition corresponding to this cloud volume is 26% H2 and 38% steam. This corresponds to the mixture most likely to detonate as determined from Fig. 1. In addition to the 15% case, volume fractions of 30%, 60%, 80%, and 100% were also examined.

In these scoping calculations, a simplified geometry representing the CE80+ containment shell, interior structures and the cloud of detonating hydrogen-air-steam mixture was used. This is (Fig. 3) just a hemisphere of hydrogen-air-steam within a hemispherical shell that represents the upper part of the containment. This one-dimensional idealization of the containment is only being used to study the effect of cloud radius on the structural loading. A range of cloud sizes (as discussed above) were examined to understand how sensitive the computed loading is to cloud size. It is important to note that only the smallest cloud size would actually be expected to detonate on the basis of the considerations given in Shepherd (1993). The larger clouds are simply too lean and dilute to plausibly result in detonations being initiated by deflagration-to-detonation transition.

3 Detonation Simulations

Detonations were simulated with the ExPac[a] program. This program solves the conservation equations of gas dynamics for one and two-dimensional geometries. In the present application, a simplified model was used for an idealized detonation wave that travels at the Chapman-Jouguet (CJ) velocity. The solution method is based on the Flux-Corrected Transport method of Boris and Book as described in Oran and Boris (1987). The code has been extensively validated against experimental data and other codes as described in Boyack et al. (1992). Separate validations against experimental data[b] were carried out in this study for the detonation of a spherical cloud of stoichiometric hydrogen-air. Good agreement was found between computed and measured pressures both inside and outside of the cloud.

Prior to carrying out the gas dynamics computations, the CJ detonation parameters were first computed with the STANJAN code of Reynolds (1986). The results of the STANJAN computations are given in Table 3 for the cloud cases given in Table 2. The detonation velocity and pressure decrease with increasing cloud volume since the concentration of hydrogen is decreasing. Detonation cell widths λ_{est} were estimated with the

[a] Available from Combustion Dynamics, Ltd, Medicine Hat, Alberta, CANADA

[b] Provided by W. Breitung of Kernforschungszentrum, Karlsruhe, Germany

ZND model and the correlations discussed in Shepherd 1993. As shown in Table 3, cases 1 and 2 have large but not unreasonable values of $\lambda_{est} = 1.6$ and 2.7 m, respectively. Since the characteristic length scale in the upper dome is 30 m, detonation of these mixtures is possible but there is still a substantial issue connected with the initiation of such insensitive mixtures. The other cases (3, 4 and 5) have extremely large cell widths and cases 4 and 5 appear to be outside the flammability limit. Detonation calculations for these cases have been included purely as an intellectual excerise and all evidence indicates that detonation would actually be impossible in these cases.

4 Results of Detonation Simulations

Simulations were carried out with the hemispherical model geometry using a mesh size of 0.05 m for a total of 510 mesh points. The total duration of the simulation was about 200 ms, enough for four cycles of shock reflection. This resulted in a total of between 7,000 and 14,000 time steps per simulation. The results of the detonation simulations are given in Figs. 4 to 18. Pressures are given as normalized values $\Delta P/P_o$ where P_o is the initial pressure of 2.37 bar. The pressure is given at two points. One point is at 10 m from the center of the hemisphere, inside the combustible cloud. The other point is on the shell, 25.5 m from the center of the hemisphere. The actual loading on the shell can be computed as

$$P_{\text{load}} = P_o \times \left(\frac{\Delta P}{P_o} + 1\right) - P_a$$

where P_a is the ambient pressure outside the shell.

The scaled impulse

$$I_{\text{scaled}} = \int_o^t \frac{\Delta P(t')}{P_o} dt'$$

is given only at the shell location, 25.5 m from the center of the hemisphere. Note that the impulses increase linearly with time, making the impulse a useless parameter for this type of explosive loading. In contrast, unconfined blast waves are usually characterized by a constant value of the impulse, (Baker et al. 1983). This is clearly not the case for internal explosions with a constant residual pressure. As discussed below, estimating structural response in the present problem is more difficult than in external blast problems due to the multiple shocks and the residual pressure.

Peak pressures at the shell are given in Table 4. Note that these pressures are quite a bit lower than what would be produced by the normal reflection of the detonation directly from the wall. This process produces a peak pressure (Shepherd et al. 1991) that is roughly 2.5 times the CJ pressures of Table 3. The lower peak pressures are due to the attenuating effects of the shock propagation through the layer of nonreactive mixture between the cloud and the shell. This attenuation is opposite to the amplification found by Boyack et al. (1992) for thin inert layers in *planar* geometries. This is due to larger thickness of our layers and a stronger attenuation effect of the expansion wave behind the shock in spherical geometries than in planar problems. Most significant, we find that

the maximum structural deflection does not occur due to the first shock wave so that the peak pressure of the first shock is not useful for characterizing the structural response.

The adiabatic constant-volume explosion pressure (AICC pressure) for all cases is the same and equal to 5 bar, i.e, this is the peak pressure that would be produced by a deflagration of these mixtures. This also corresponds to the idealized residual pressure that will exist after all the transient waves have decayed. This residual pressure can be clearly observed in Fig. 17 and is responsible for the linear increase of impulse with time.

The computation can be divided into two stages. In the first stage, the detonation wave propagates through the combustible part of the mixture, the "cloud." The detonations were initiated (at time $t = 0$) at the center of the combustible cloud (Fig. 3) and propagated outward to the cloud boundary. In the second stage, waves are generated when the detonation reaches the cloud boundary. A shock wave will propagate outward toward the containment wall and a secondary wave propagates inward toward the center of symmetry. These waves then undergo further interactions with the center of symmetry (an implosion process) and reflection from the walls and the product-atmosphere interface The result of all of these interaction processes is a quasi-periodic series of pressure pulses inside the containment shell. This has been previously studied (Shepherd et al. 1991) in the case of detonation in a hemispherical container. The pressure signals in the present simulations are similar to the previous results but additional waves are present in cases 1 to 4.

5 Structural Response

The elastic response of the steel shell to computed transient pressure loads was estimated using a single degree-of-freedom model for the radial oscillations of the shell. The linear radial response equation (Baker et al. 1983) was numerically integrated with Euler's method using as parameters a shell radius of 30.8 (m) (100 ft), thickness of 44.5 mm (1.75 in), a modulus of 2×10^{11} kg·m^{-1}·s^{-2}, a Poisson's ratio of 0.3 and a density of 8.3 $\times10^{3}$ kg·m^{-3}. The computed pressures at 25.5 m (the shell location) were used as numerical inputs for the internal pressure on the shell. This calculation is highly idealized, ignoring factors such as the constraint of the concrete base that the lower portion of the shell is embedded in and the various penetrations through the shell.

The results are given in Table 3 for the maximum radial deflection u_{max}, tangential stress σ_{max}, and equivalent maximum static pressure P_{equiv}. The time t_{u-max} is the time at which the maximum deflection (and tangential stress) occur. The time histories of the radial deflections are given in Figs. 19 and 20.

One of the important conclusions of the present study is that the peak deflection and stress do not occur just after the first shock wave. Inspection of Table 4, Figs. 19-20 and comparison with the pressure traces Figs. 5,8,11,14, and 17 reveals that in all cases except 2, the peak deflection occurs just after the second shock wave at about 80 ms. In case 2, the most severe case in the present study, the peak deflection occurs at 172 ms, after the fourth (the third wave is actually split into two smaller waves) shock wave at 150 ms.

The delayed occurrence of the peak deflection is due to the relative spacing of the shocks and the structural oscillations. The fundamental period of the structure is about 23 ms (corresponding to a resonant frequency of 43 Hz) and shocks are spaced about 30 to 40 ms apart. The first shock wave sets the shell into oscillatory motion at this frequency and the possibility then exists that the secondary shock waves will arrive at the shell in a fashion that reenforces that amplitude of the deflection. This is illustrated in Fig. 19 for case 2. The bulk of the deflection appears to be caused by the first and second shock waves. In addition, the residual pressure results in a constant displacement that adds to the dynamic displacement caused by the shock waves. The initial pressure of 2.37 bar results in a static deflection of 4.8 mm prior to the test and the residual pressure of 5 bar due to the constant volume nature of the process results in a deflection of about 15 mm. We conclude that for this type of internal blast loading process that the details of structural response are very significant and that the simple estimation techniques based on peak pressure and impulse developed for external blast are not applicable.

The pressure in the last column is the key result of this analysis. This pressure should be compared to the ultimate capacity of the shell to judge wether yielding will occur or not. Based on the information in Jacob *et al.* (1993), the shell has an ultimate capacity of 12.8 bar (absolute) at 394 K. It is important to note that this is not the failure point but simply an arbitrary choice based on a strain of $\epsilon = .003$. Tensile failure of the shell material (SA357) is not expected until 88 bar or a strain of $\epsilon = .02$. Our analysis predicts that significant yielding would only occur for case 2 and even in that instance, the amount of permanent deformation would be modest.

6 Summary

One-dimensional detonation simulations and simplified structural response computations have been carried out to assess the significance of the detonation of local regions of the CE80+ containment. For a cloud size that is 15% of the upper dome volume and computed SB LOCA conditions, the first reflected shock results in a peak pressure of 8.6 bar on the containment when the initial containment pressure of 2.37 bar is accounted for. The peak reflected pressure increases as the cloud size is increased, up to a maximum value of 14.4 bar for a cloud that occupies the entire hemisphere modeling the upper dome of the containment.

The ultimate capacity of the shell has been estimated to be 12.8 bar at a temperature of 393 K. The equivalent static pressures computed from the single-degree-of-freedom structural model are comparable to this pressure except in case 2, which had an equivalent static pressure of 19.2 bar. However, even in this case, only a modest amount of permanent deformation would be expected since tensile failure is not expected until a static pressure of 88 bar.

We conclude that:

- Local detonations with realistic quantities of hydrogen produce structural loads that are comparable with the ultimate capacity but far below the tensile failure

limit of the steel shell.

- The interaction of the detonation with the cloud boundary and the decay of the shock wave due to the expansion wave are significant in determining peak pressures and structural deflections. An optimum cloud size appears to exist for generating the maximum deflection of the structure.

- The maximum deflection occurs due the interaction of the secondary shock waves with the structural oscillations.

Finally, these computations indicate that computing structural deformation from blast loading can involve subtle effects that requires careful evaluation. Simple engineering correlations developed for external blast must be used very cautiously. If more realistic computations with multidimensional geometries are used for the gas dynamic portion, there should be a comparable increase in the sophistication of the structural computation.

7 References

1. W. E. Baker, P. A. Cox, P. S. Westine, J. J. Kulesz, R. A. Strehlow **Explosion Hazards and Evaluation**, Elsevier, 1983.

2. Boyack, K. W., Tieszen, S. R., Stamps, D. W. *Loads From the Detonation of Hydrogen-Air-Steam Mixtures* Sandia National Laboratories Report, SAND92-0541, 1992.

3. Jacob, M. C., Schneider, R. E., and Finnicum, D. J. "System 80 Design Features for Severe Accident Prevention and Mitigation", ASME-JSME Nuclear Engineering Conference - Vol. 1, pp. 367–389, 1993.

4. E. Oran and J. P. Boris **Numerical Simulation of Reactive Flow**, Elsevier, NY, 1987, p. 275.

5. Reynolds, W. C. *The Element Potential Method for Chemical Equilibrium Analysis: Implementation in the Interactive Program STANJAN, Version 3*, Dept. of Mechanical Engineering, Stanford, CA, January 1986.

6. J. E. Shepherd, A. Teodorczyk, R. Knystautas, and J. H. Lee, "Shock Waves Produced by Reflected Detonations," *Progress in Astronautics and Aeronautics* **134**, 244-264, 1991.

7. Shepherd, J. E. *Hydrogen Combustion and Explosion during Severe Accidents in Nuclear Power Plants*, draft report to the US NRC, June 21, 1993.

Table 1. Well-Mixed Conditions during a Small-Break LOCA.

Species	Mole %
H2	5.0
O2	9.6
CO	1.5
H2O	47.8
N2	36.1

Table 2. Cloud Parameters.

Case	volume fraction	Radius (m)	(ft)	X_{H_2}	X_{N_2}	X_{O_2}	X_{H_2O}
1	0.15	13.6	44.6	0.260	0.2812	0.0748	0.384
2	0.30	17.1	56.1	0.150	0.3233	0.0859	0.441
3	0.60	21.5	70.5	0.081	0.3492	0.0928	0.478
4	0.80	23.7	77.7	0.062	0.3563	0.0947	0.487
5	1.00	25.5	83.7	0.050	0.3610	0.0960	0.493

Table 3. Detonation Parameters.

Case	U_{CJ} (m/s)	P_{CJ} (bar)	T_{CJ} (K)	ρ_{CJ} (kg/m^3)	γ_{CJ}	λ_{est} (m)
1	1719.	17.8	1899.	2.19	1.232	1.6
2	1595.	17.5	1858.	2.48	1.222	2.7
3	1261.	11.9	1270.	2.55	1.260	>100
4	1142.	10.1	1086.	2.54	1.275	>100
5	1066.	8.90	977.	2.52	1.286	>100

Table 4. Shell Loading and Structural Response Estimates

Case	P_{max} (bar)	u_{max} (mm)	σ_{max} (MPa)	t_{u-max} (ms)	P_{equiv} (bar)
1	8.6	39.	364.	82.	11.6
2	12.5	66.	624.	77.	19.2
3	13.5	46.	430.	77.	13.5
4	13.9	41.	390.	172.	12.3
5	14.4	42.	395.	80.	12.5

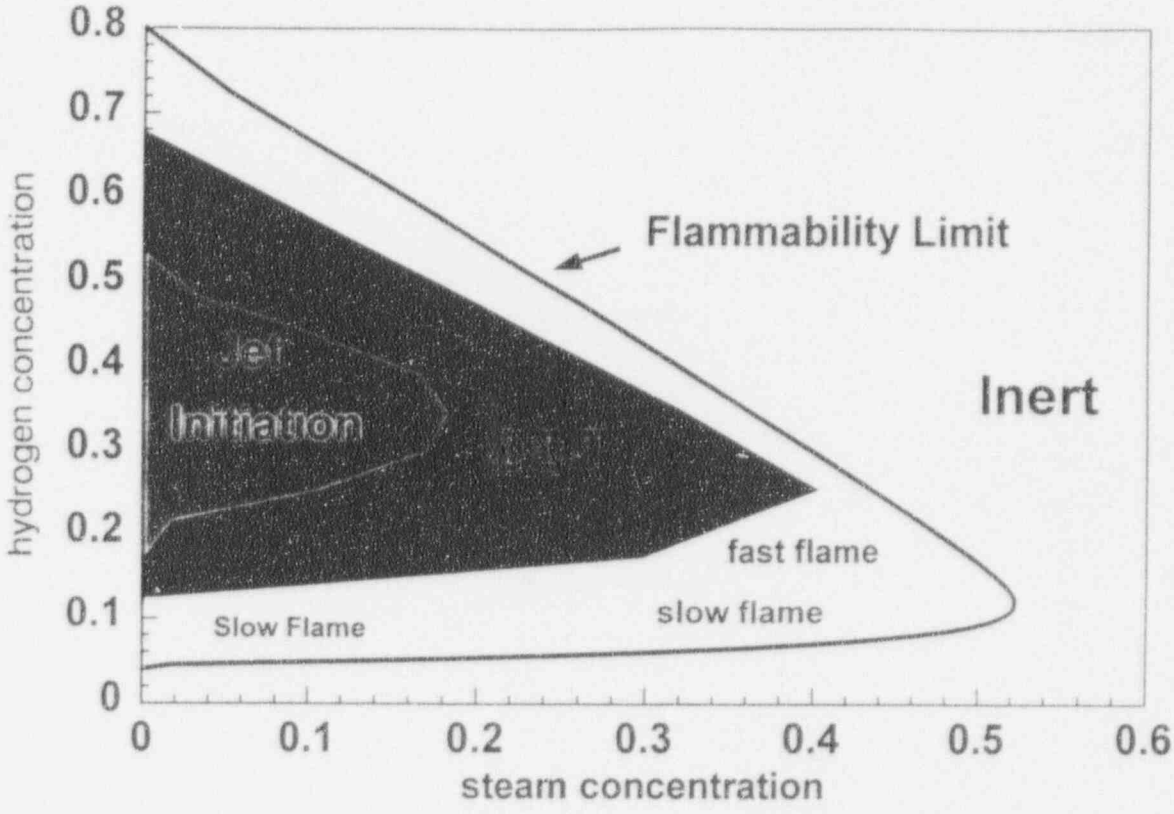

Figure 1. Combustion regimes in hydrogen-air-steam mixtures(Shepherd 1993).

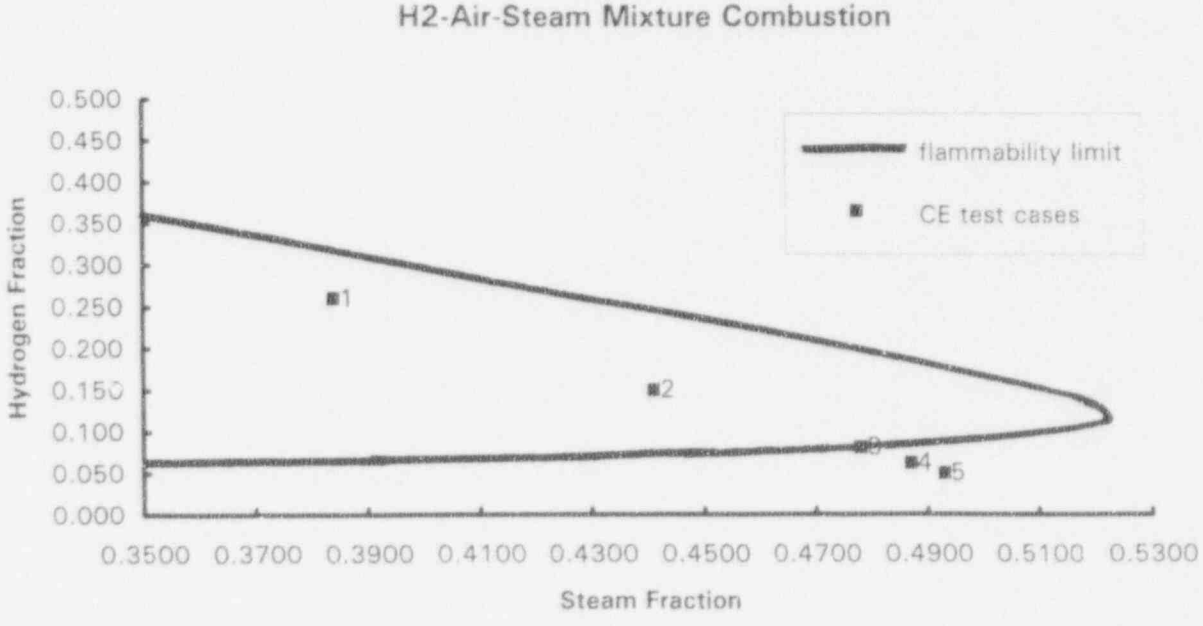

Figure 2. Cloud composition and flammability limit for theCE80+ scoping study.

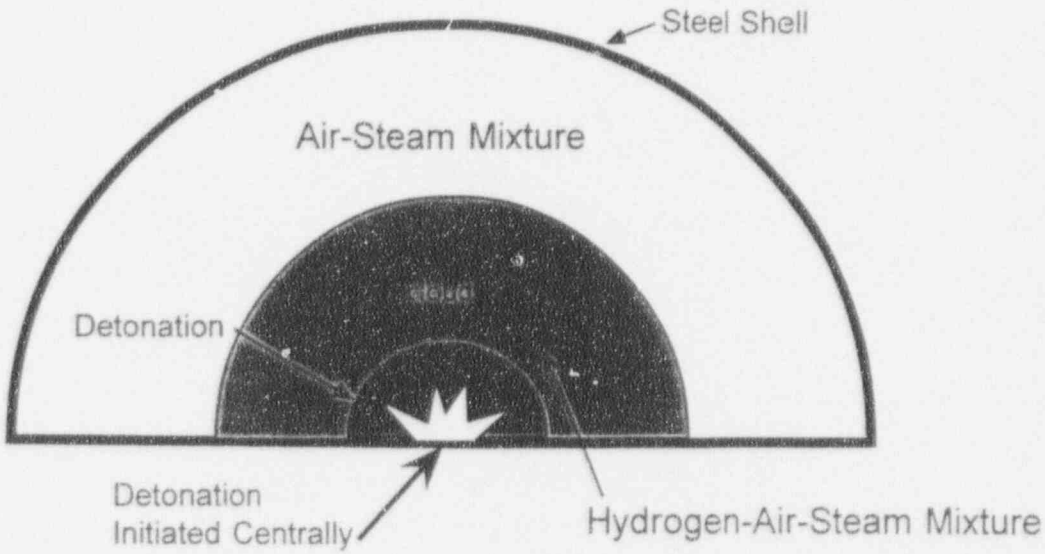

Figure 3. Simple model geometry used to study the effect of cloud size in theCE80+ upper dome.

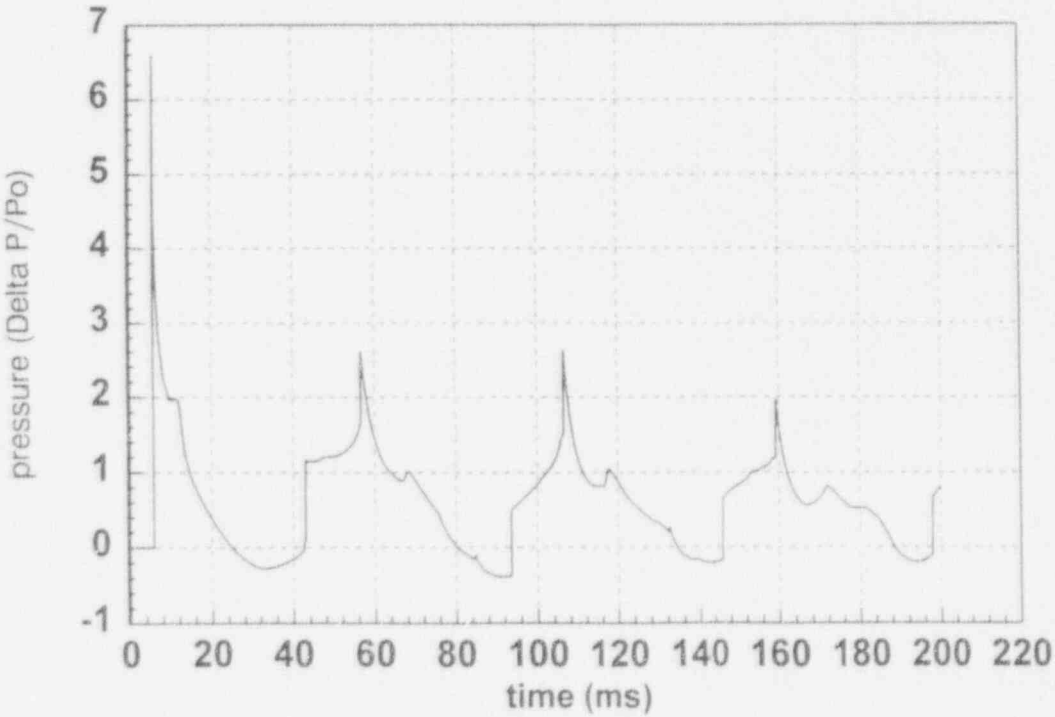

Figure 4. Case 1. Pressure vs. time at 10 m distance (insidecloud).

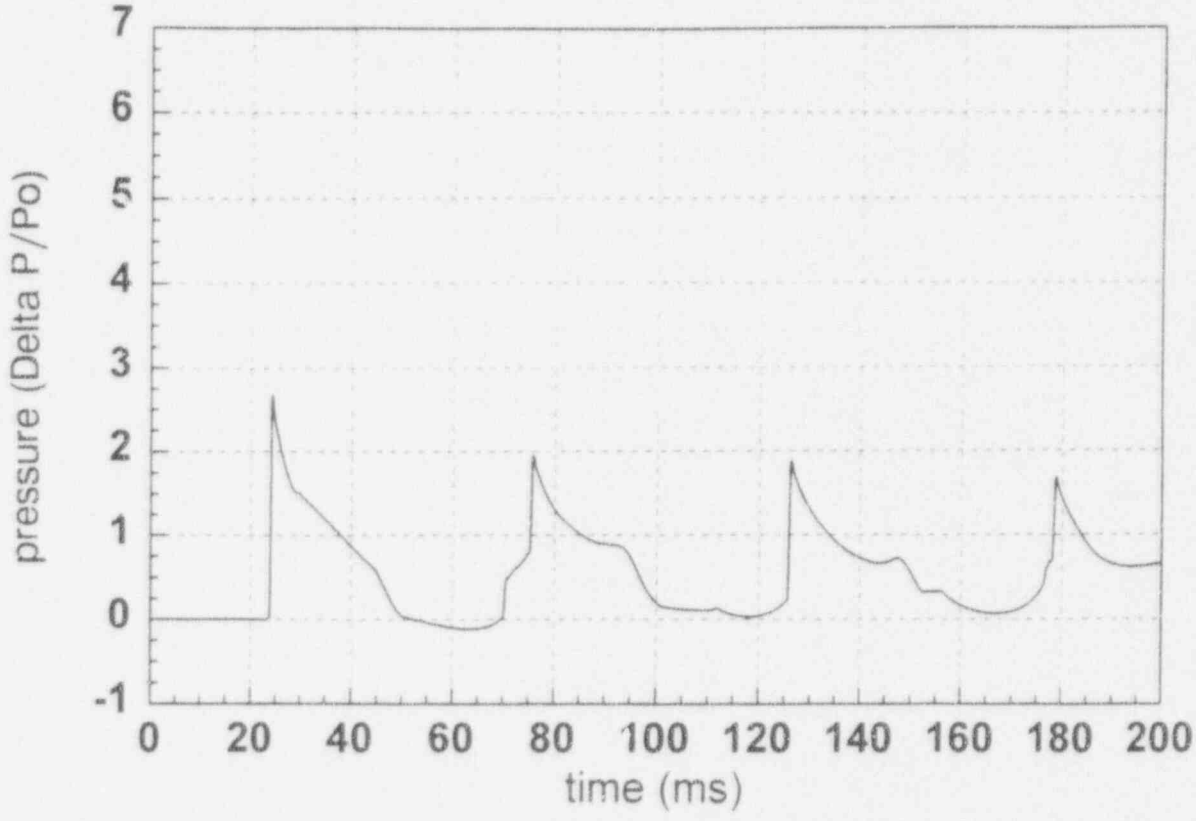

Figure 5. Case 1. Pressure vs. time at 25.5 m distance (shell).

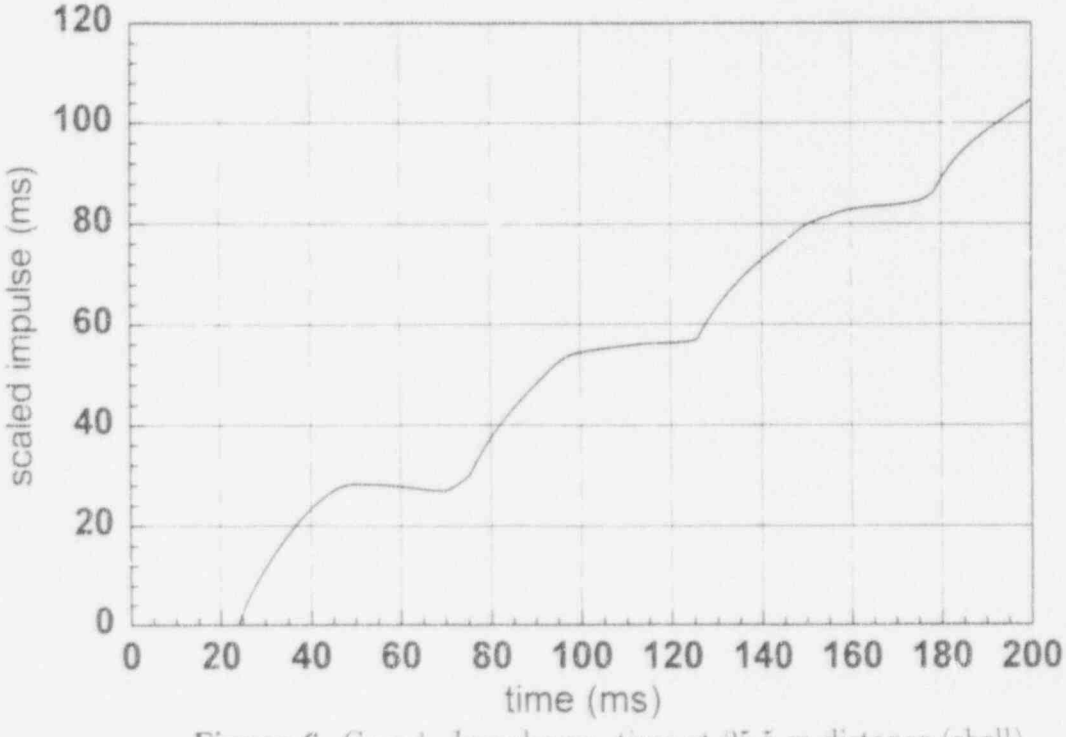

Figure 6. Case 1. Impulse vs. time at 25.5 m distance (shell).

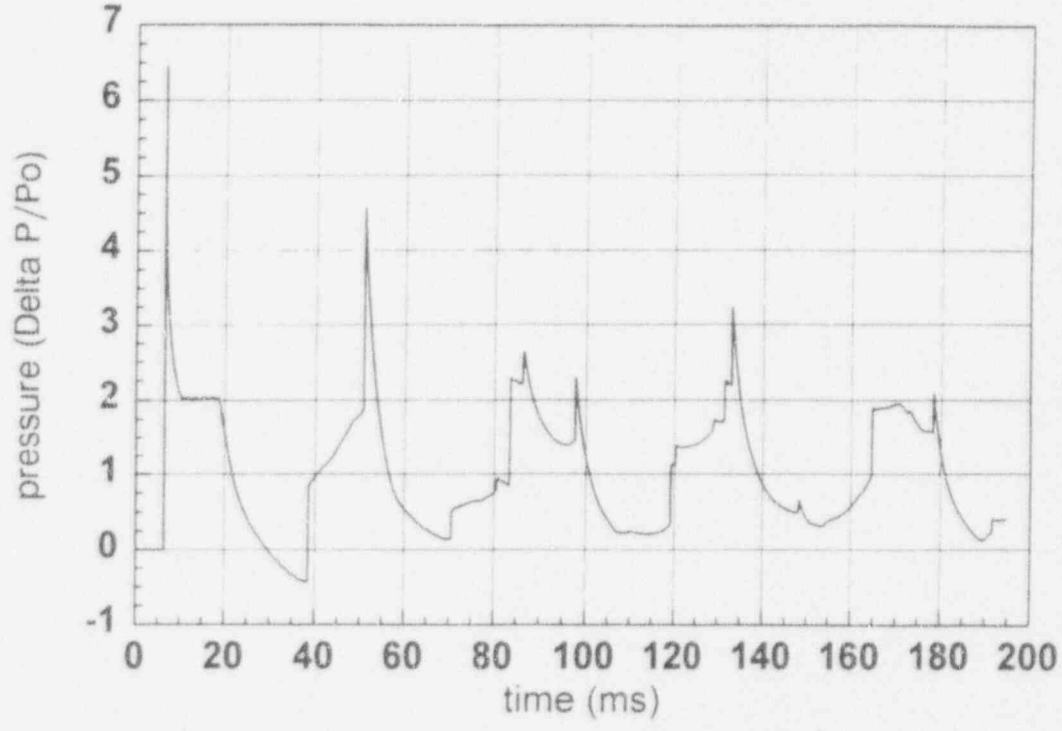

Figure 7. Case 2. Pressure vs. time at 10 m distance (insidecloud).

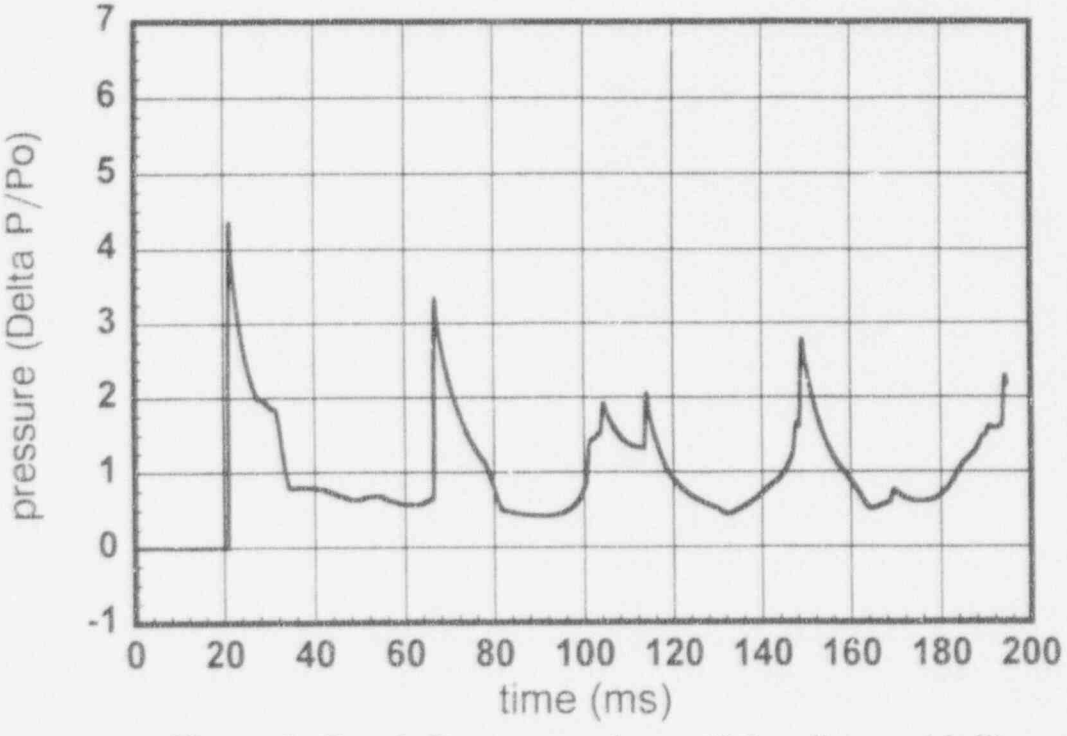

Figure 8. Case 2. Pressure vs. time at 25.5 m distance (shell).

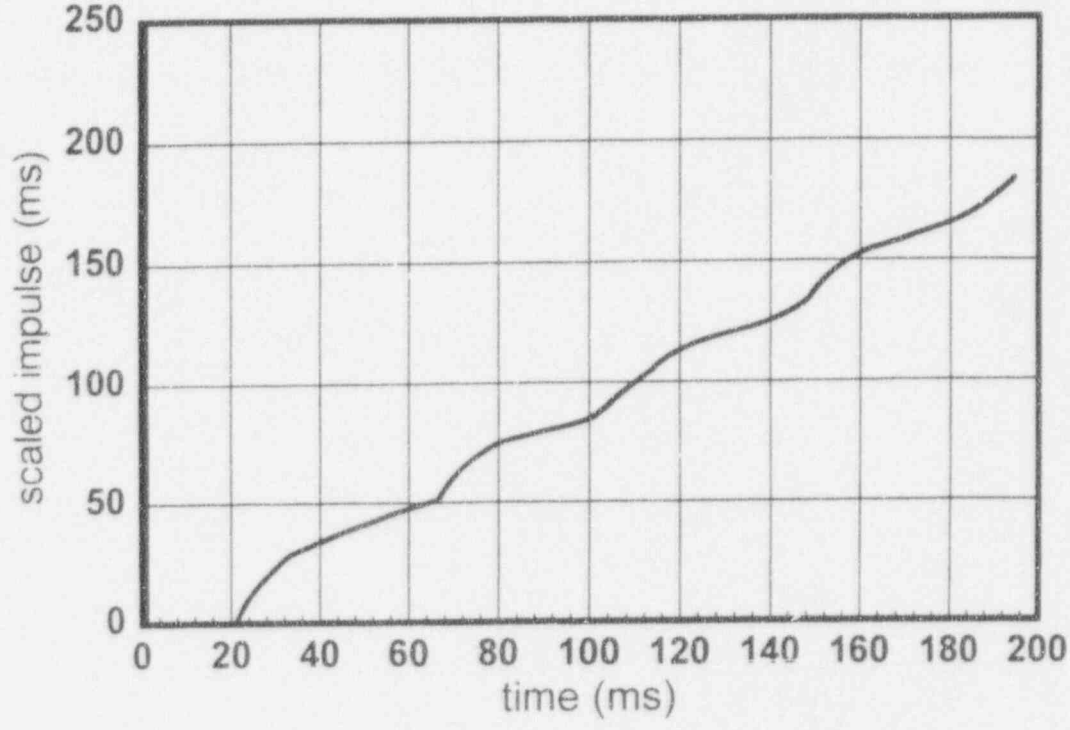

Figure 9. Case 2. Impulse vs. time at 25.5 m distance (shell).

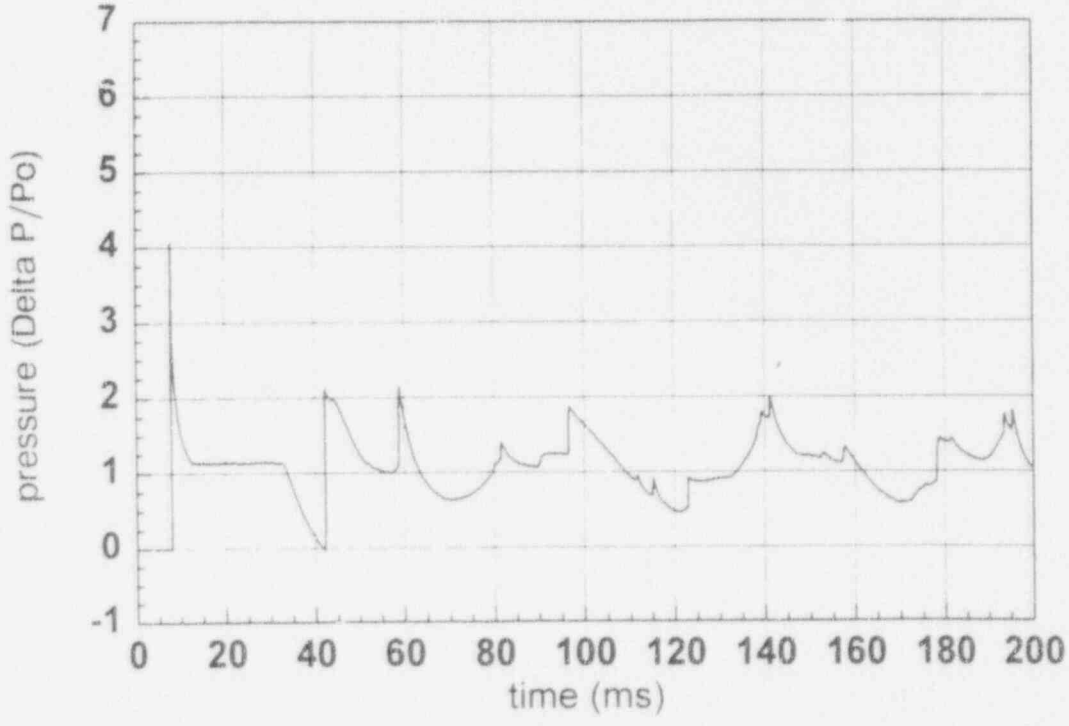

Figure 10. Case 3. Pressure vs. time at 10 m distance (inside cloud).

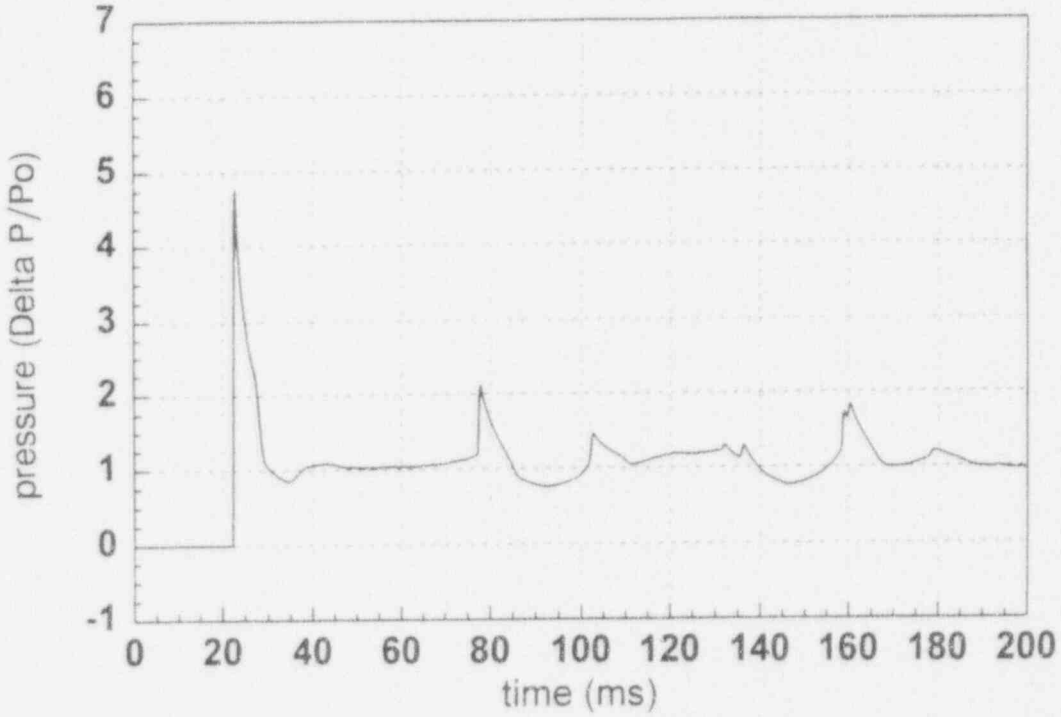

Figure 11. Case 3. Pressure vs. time at 25.5 m distance (shell).

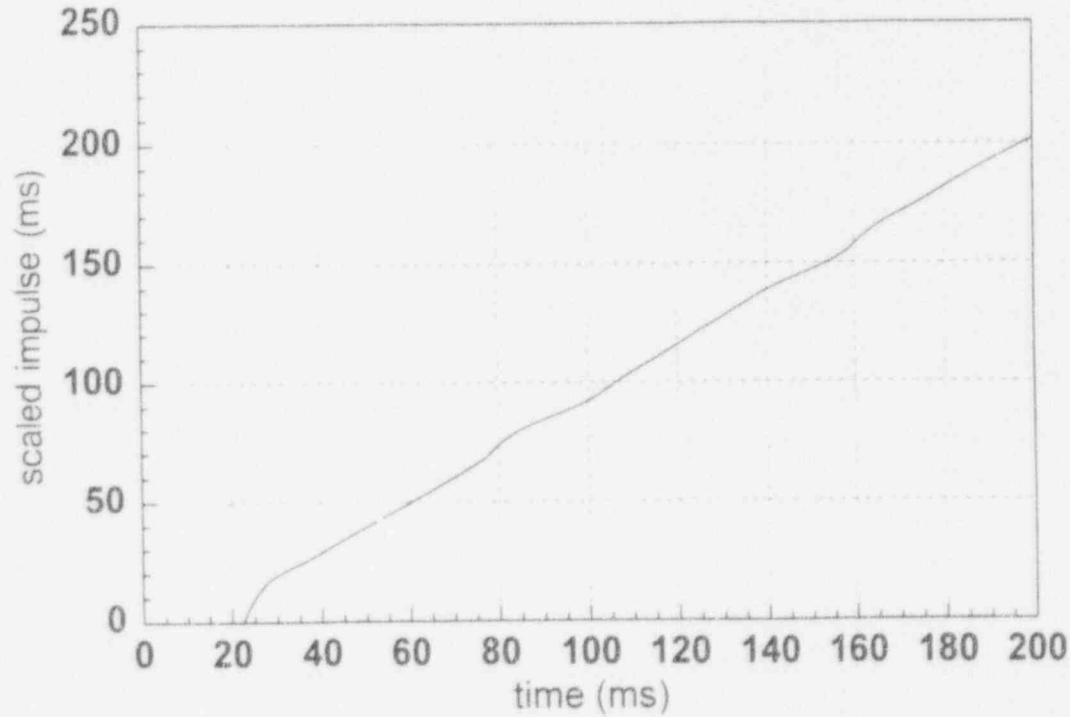

Figure 12. Case 3. Impulse vs. time at 25.5 m distance (shell).

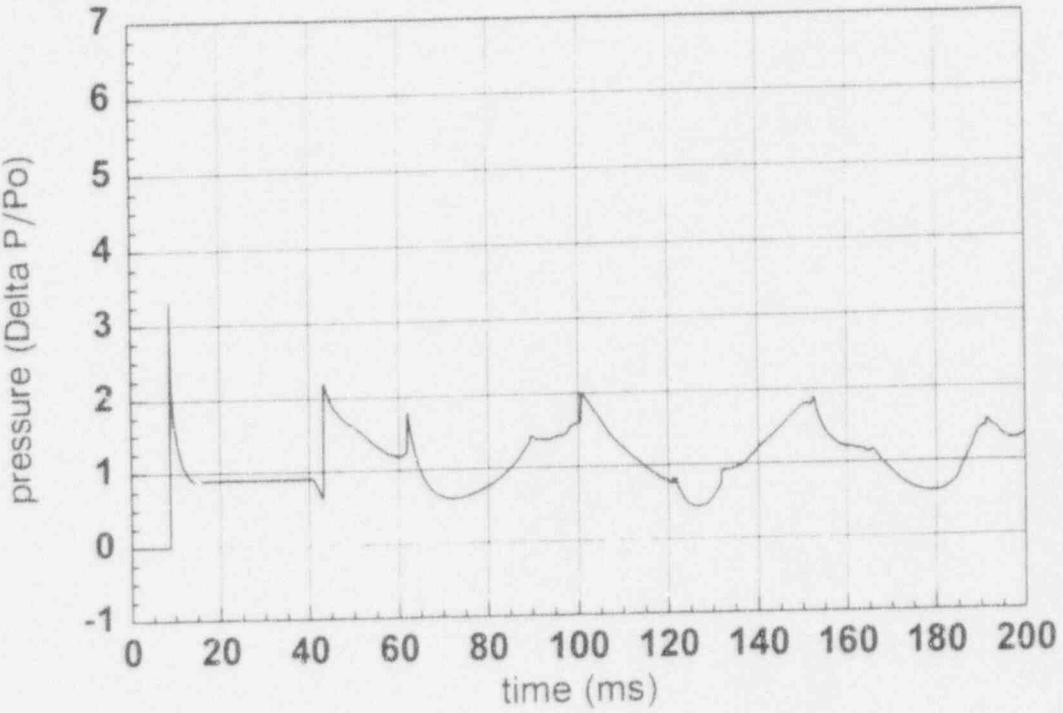

Figure 13. Case 4. Pressure vs. time at 10 m distance (inside cloud).

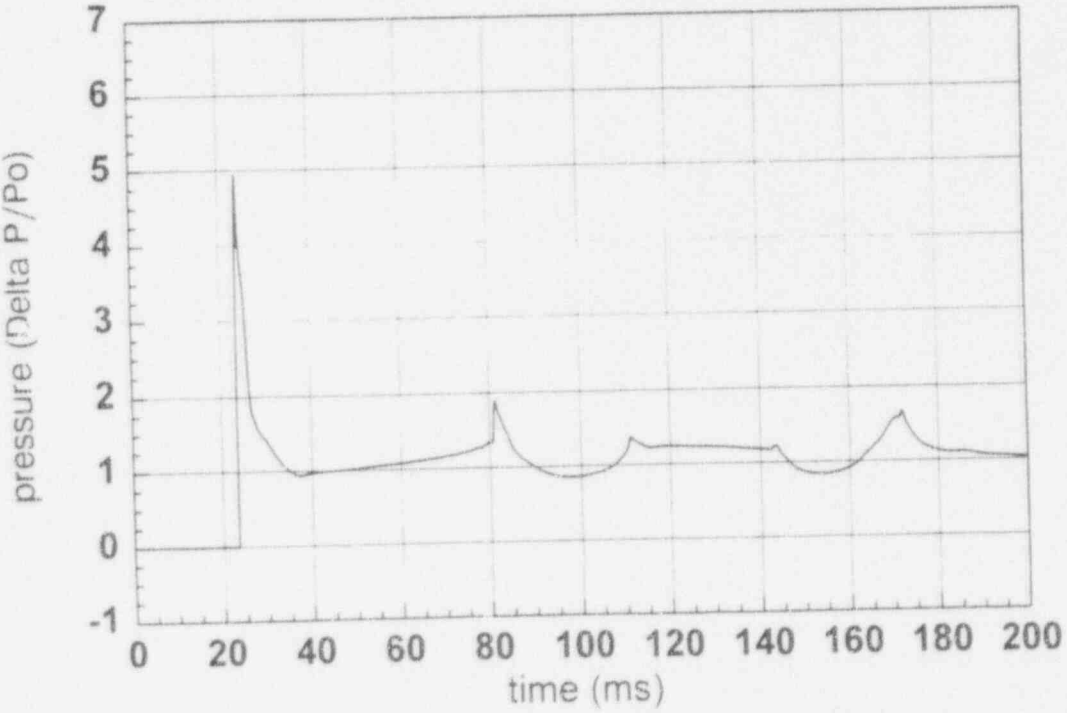

Figure 14. Case 4. Pressure vs. time at 25.5 m distance (shell).

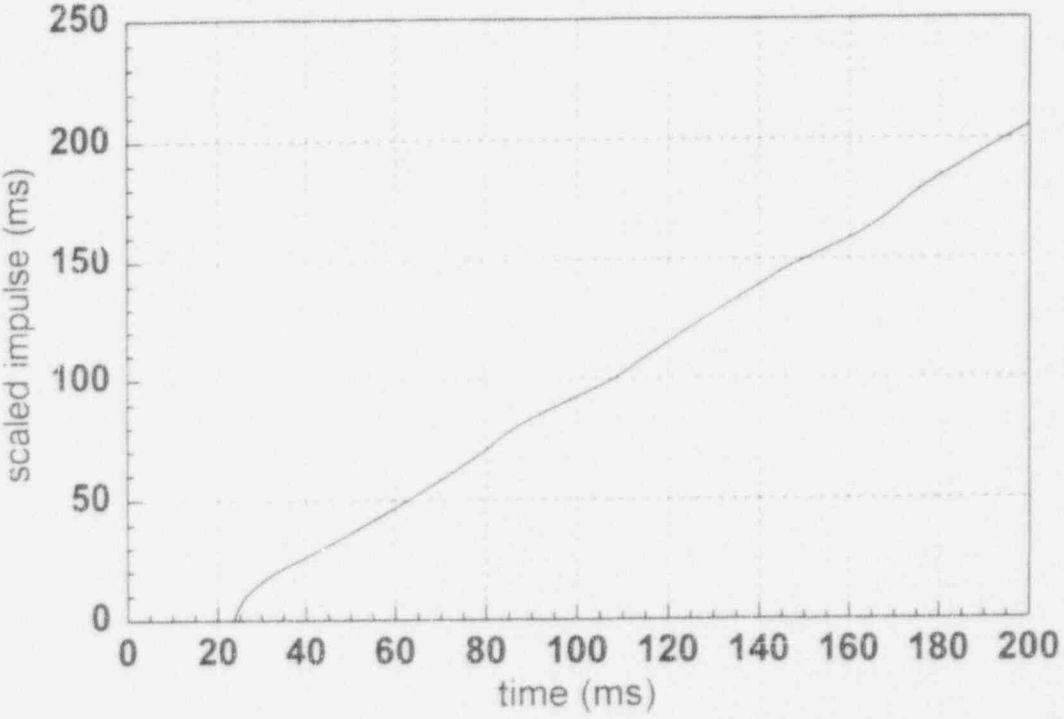

Figure 15. Case 4. Impulse vs. time at 25.5 m distance (shell).

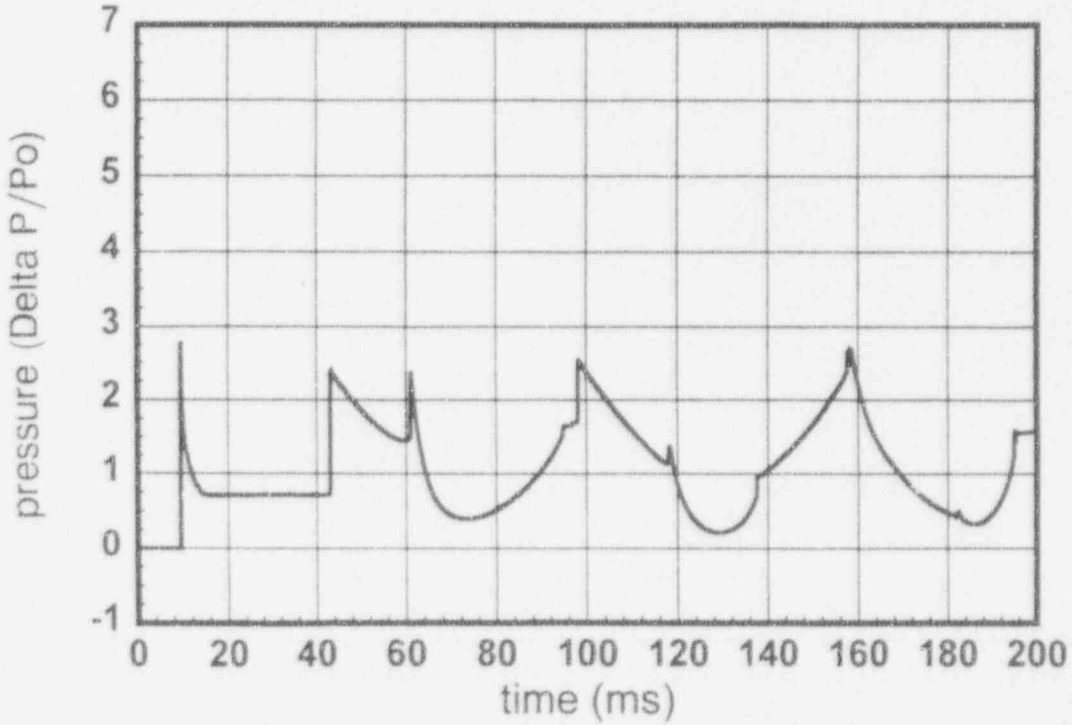

Figure 16. Case 5. Pressure vs. time at 10 m distance (inside cloud).

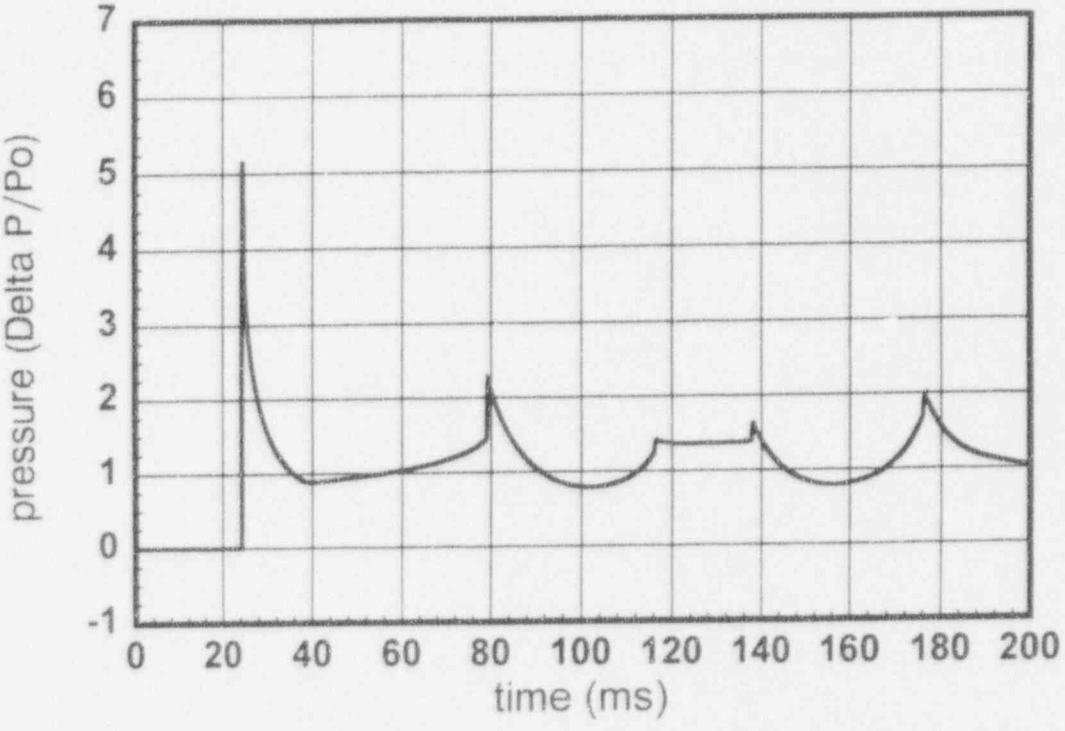

Figure 17. Case 5. Pressure vs. time at 25.5 m distance (shell).

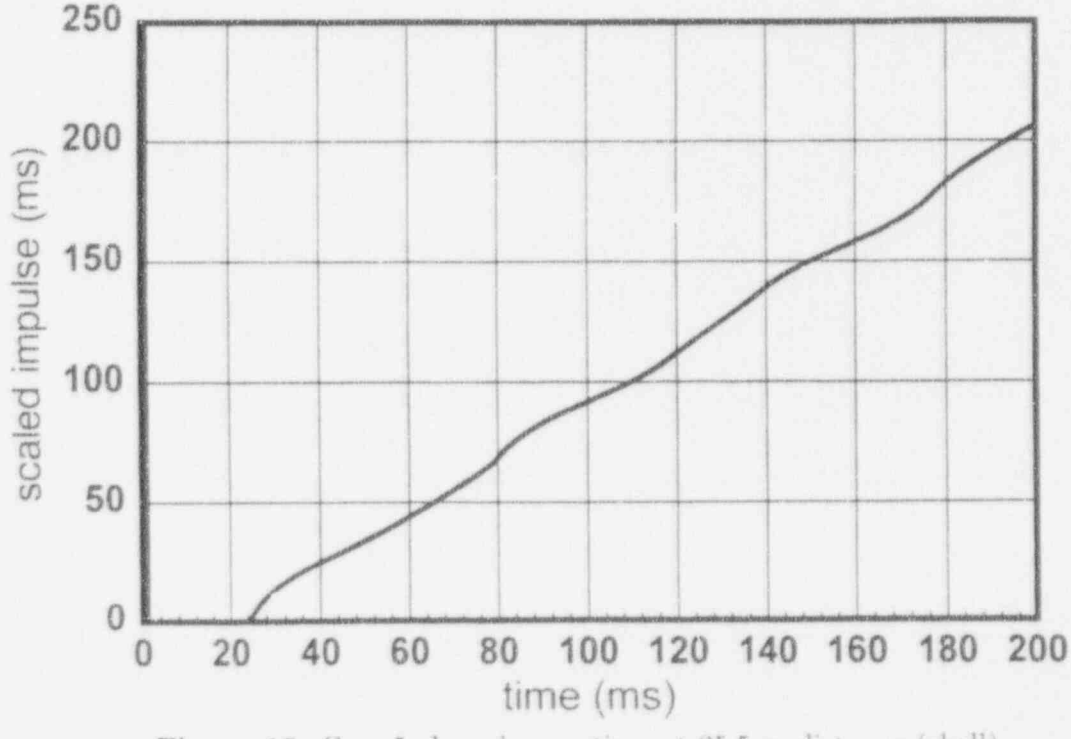

Figure 18. Case 5. Impulse vs. time at 25.5 m distance (shell).

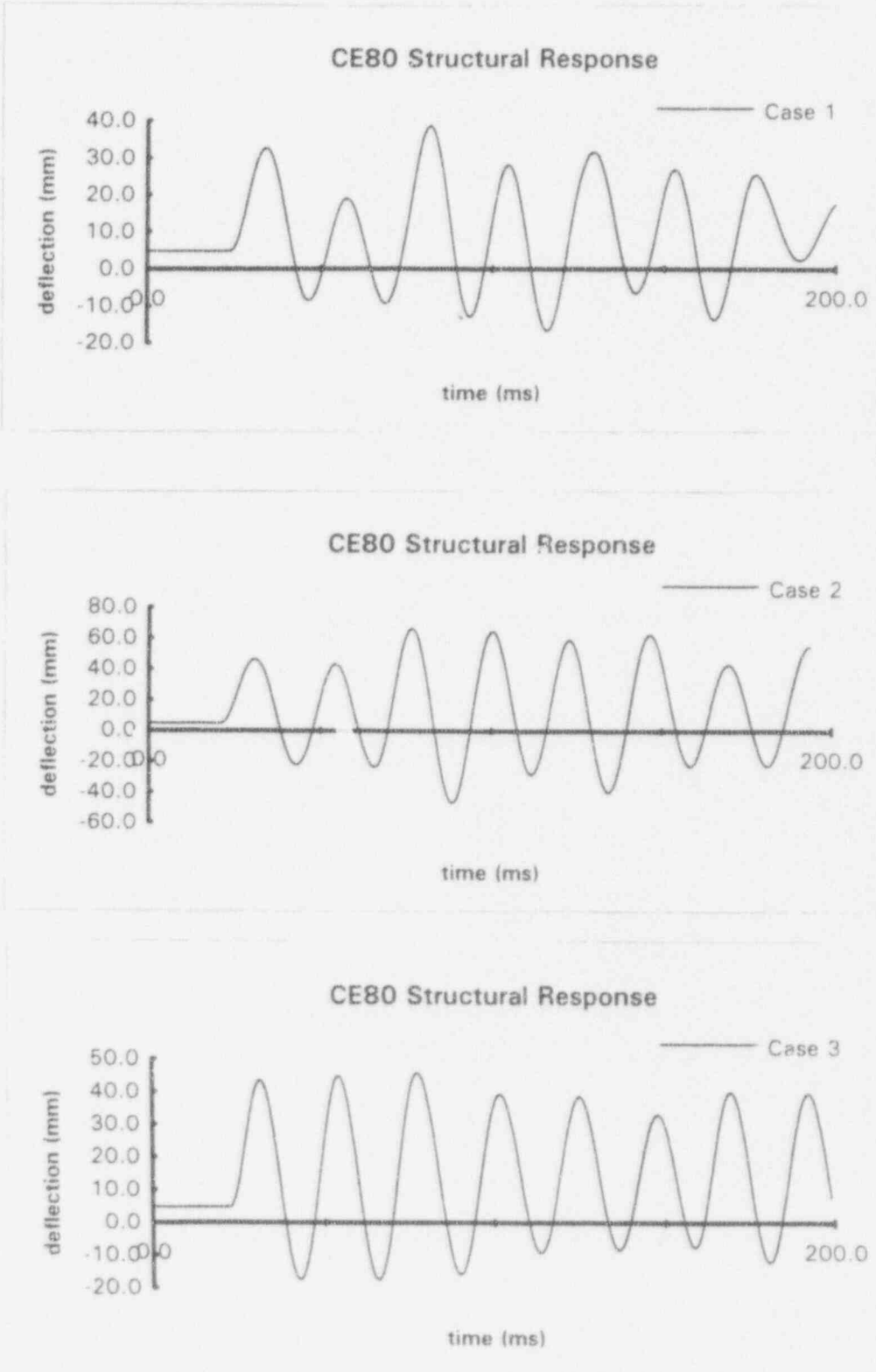

Figure 19. Radial deflection vs. time for cases 1, 2 and 3.

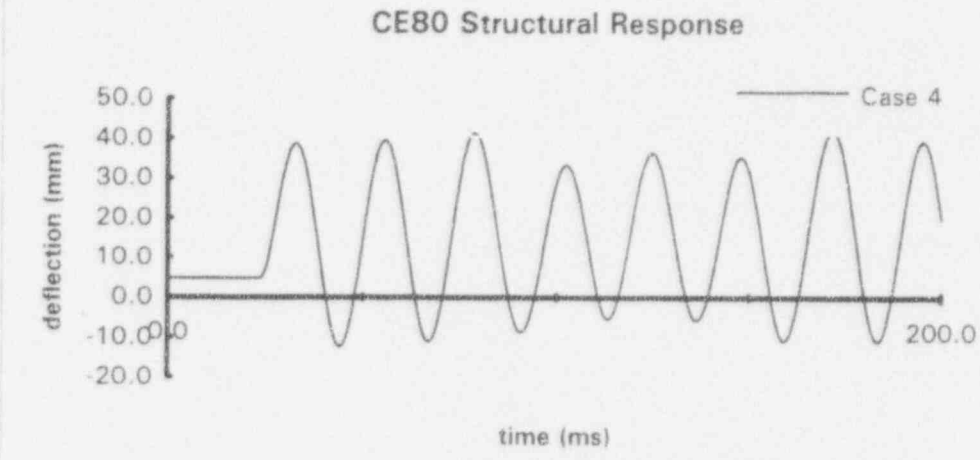

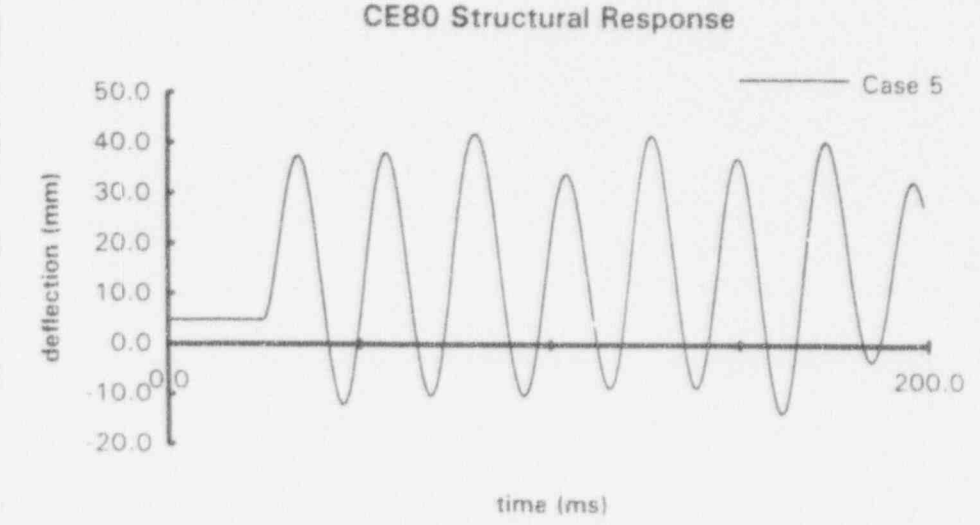

Figure 20. Radial deflection vs. time for cases 4 and 5.

ENERGY RESEARCH, INC.

P.O. Box 2034
Rockville, Maryland 20847
(301) 881-0866 / FAX 881-0867

June 14, 1994

Drs. S. Abdel-Khalik and S. M. Ghiaasiaan
3579 Midvale Cove
Tucker, Georgia 30084

Subject: **"Analysis of Ex-Vessel Steam Explosions for the Combustion Engineering System 80+ Using the GT3F™ Computer Code," (June 1994).**

Dear Drs. Abdel-Khalik and Ghiaasiaan:

Thank you for your letter of June 3, 1994 and the subject letter report containing the results of your GT3F™ computer code calculations.

Dr. H. Esmaili of my staff has now completed his review of the subject document (please refer to the attached memorandum), and several issues/questions remain to be addressed at your earliest convenience, in order to close-out the ERI Work Orders for these calculations.

Please feel free to call me or Dr. Esmaili, if you have any questions.

Sincerely,

Mohsen Khatib-Rahbar

Attachment: H. Esmaili,"CE System 80+ Ex-Vessel Calculations Using GT3F™ Computer Code," Memorandum (June 13, 1994).

cc: A. Behbahani, NRC